Motion Artefacts Modelling in the Application of a Wireless Electrocardiogram

Waltenegus Dargie[1]

***Abstract*— Wireless electrocardiograms can be useful for a wide range of applications including early detection of seizures onset, West Syndrome, sleep apnoea, Temporal Lobe Epilepsy (TLE), supra-ventricular tachycardia, atrial flutter, and atrial fibrillation. One of the advantages of using wireless sensing platforms in telemedicine is that patients can freely move and carry out everyday activities unhindered whilst vital cardiac action potentials are being measured. However, the measurements are highly sensitive of motion as motion changes the electrical interface between the electrodes and the skin and, thereby, distorts the useful signal. In this paper we propose a strategy for establishing the statistics of motion artefacts. Our approach employs 3D accelerometers to reason about the movement affecting the electrodes of a wireless electrocardiogram and takes advantage of the structure and sequence of cardiac action potentials.**

***Index Terms*— Accelerometer, wireless electrocardiogram, cardiac action potential, telemedicine, mean square error estimation, inertial sensor, noise, estimation**

I. Introduction

Bio-potential signals which can be sensed from different parts of the human body reveal vital underlying physiological and psychological conditions and are routinely used to diagnose and monitor a large number of diseases [1], [2]. These signals can be sensed by strategically placing pairs of electrodes on the surface of the skin or implanting them. For examples, an electrocardiogram is used to sense cardiac bio-potentials; an electroencephalograph, to sense the electrical activities of the brain, and an electromyogram, to sense the bio-potentials generated by the contraction and relaxation of the muscles. Traditionally, these devices have been used in clinical settings for short-term diagnosis and monitoring because they are bulky and power consuming and require controlled environments to function properly.

More recently, wireless bio-potential sensors have been developed both by the research community and the industry, initial results suggesting the affordable, unobtrusive, and ubiquitous usage in rehabilitation as well as residential settings [3], [4], [5], [6], [7], [8]. The prevailing design goals have been achieving small form-factors, small weight, high energy-efficiency, bidirectional wireless communication, remote and dynamic reprogramming and reconfiguration, adaptive sampling, and local signal processing. These features will be useful to deploy the sensors on the bodies of patients who can freely move and carry out everyday activities whilst vital bio-potential signals are being sensed. This way, the possibility of predicting the onset of diseases or observing symptoms which may otherwise remain hidden during clinical diagnosis increases considerably. Furthermore, the monitoring task (durations, intervals, and rates) can be remotely controlled and adapted to the need of individual patients and communication bandwidth and local computational resources can be used efficiently. However, the use of wireless sensing platforms presently poses some formidable challenges, one of these being the inclusion of motion artefacts during mobility [9], [10], [11]. Partly due to the undesirable vibration of electrodes and partly due to the change in the electrical characteristics of the skin, these movement artefacts significantly distort the useful signal.

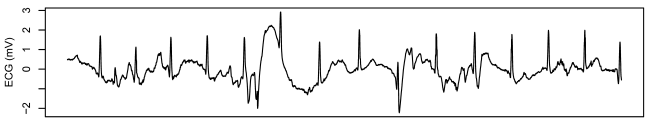

Fig. 1: The cardiac action potentials of a healthy subject climbing up a staircase at a normal pace. The measurement was obtained from a wireless electrocardiogram.

Fig. 1 displays a snapshot of the measurement we took with a 5-lead wireless electrocardiogram (the Shimmer platform [6]) whilst a healthy adult person was climbing up a staircase at a normal pace. In a healthy person, the electrocardiogram measures a sequence of three essential waves – the P, the QRS, and the T waves – revealing vital underlying cardiac states (ref. to Fig. 2 for a detailed description of the electrocardiogram measurement of a healthy person). The frequency of these waves, their chronological appearance, and the interval between them are critical to interpret the electrocardiogram.

In this paper we demonstrate how we modelled the statistics of motion artefacts using inertial sensors. We deployed a 3D accelerometer near the electrodes of a wireless electrocardiogram to measure the movements affecting its electrodes and attempted to establish correlation between the measurements we obtained with the accelerometer and the movement artefacts included in the ECG measurements. We regarded different types of everyday movements – walking, running, cycling, and climbing up and down a stair case – and initial results suggest that indeed correlations can be established and the noise statistics can be estimated. We assert that the insights we obtained can be useful to identify the optimal estimator for removing motion artefacts.

[1]Waltenegus Dargie is with the Chair of Computer Networks, Faculty of Computer Science, Technical University of Dresden, 01062, Germany waltenegus.dargie@tu-dresden.de

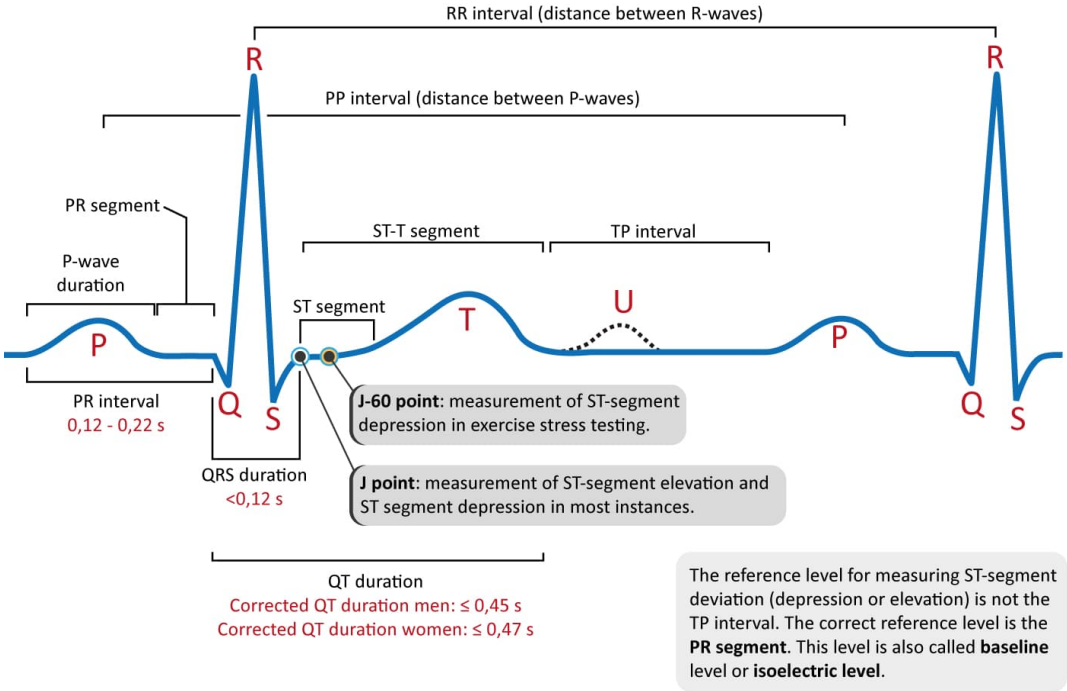

Fig. 2: Cardiac action potentials revealing underlying cardiac activities. In a normal human being, the intervals between a P-wave and a QRS-wave complex, a QRS-wave complex and a T-wave and a T-wave and a P-wave have zero or approximately zero potentials (Courtesy to Dr. Araz Rawshani, MD, PhD, 2017).

The remaining part of this paper is organised as follows: In Section II, we review related work. In Section III, we set the prerequisite for estimating the motion artefacts included in the measurements of a wireless electrocardiogram using inertial sensors. In Section IV we propose an approach for estimating the statistics of motion artefacts. In Section V, we estimate motion artefacts using the measurements of a 3D accelerometer and a linear least mean square error estimation. Finally, in Section VI, we give concluding remarks.

II. Related Work

Different researchers have in the past attempted to model motion artefacts. Tong et al. [12] embedded a 3D accelerometer and a two-axis Anisotropic Magnetoresistive (AMR) sensor into one of the electrodes of an ECG. In order to reason about motion artefacts, they deliberately induced motion artefacts by:

1) pushing on the electrode,
2) pushing on the skin around the electrode, and
3) pulling on the electrode lead wire.

This way, the authors acquire five datasets for each experiment they undertook: (1) a dataset without any induced motion, (2) a dataset containing noise induced by each of the above three methods, and (3) a dataset containing both the noise-free segments and the noise induced by all the three methods. The measurements of the ECG, the 3D accelerometer, and the AMR were synchronised. The authors evaluated the contribution of the motion sensors in cleaning the noisy signal by evaluating the L2 norm, the MaxMin statistic, and a percent improvement statistic. The noise-free dataset was used as the "ideal" reference signal. The authors claimed that there were indeed strong correlations between the motion artefacts and the outputs of the motion sensors in all the test cases. Moreover, compared with the measurements obtained by the AMR sensor, the measurements of the 3D accelerometers exhibited stronger correlations. The authors emphasised that the accelerometer was able to capture the 3-dimensional movements of the electrode whilst the AMR could only measure the 2-dimensional movements. Secondly, the relationship between the accelerometer measurements and the motion artefacts was better modelled by a linear time-varying system. However, the movement types Tong et al. considered were elementary and were carried out in a controlled environment. By contrast, we investigated the effect of motion artefacts during free movements.

Romero et al. [13] attempted to estimate the effect of motion artefacts by measuring the change in the impedance of the interface between the skin and the electrodes of a wireless ECG. This impedance is modelled as a series resistive load and a voltage source connected to a parallel RC circuit. In order to measure the change in the impedance, the authors integrated both AC and DC current sources into the wireless ECG they developed. The current sources inject a small amount of current into the body and, then, the voltage across the electrode-skin impedance is measured.

In order to examine the existence of correlations between the impedance voltage (representing motion) and the motion artefacts included in the ECG measurements, the authors

deployed four electrodes at the back of a subject, at the height of the lumbar curve, where ECG signals were expected to be negligible – two of the electrodes measured the action potentials arising from motion and the other two measured the change in the impedance voltage arising from the change in the skin-electrode interface. Ten subjects were involved in the experiment and 25 datasets were obtained. The test results indicate that there were correlations between the motion of the users and the motion artefacts but the strength of these correlation was dependent on the signal-to-noise ratio of the noisy ECG signal. The disadvantage of this approach is the injection of an extra current into the human body, however small its magnitude.

De Luca et al. [14] use uniaxial accelerometers to model and remove movement artefacts from the measurements of a surface-electromyogram. Thus, they deployed the accelerometers at different locations in the body, including the Tibialis Anterior (TA) and First Dorsal Interosseous (FDI) muscles, to capture normal and shear accelerations and the long-term drift in the EMG measurements. The measurements from the EMG and the accelerometers were obtained while the subjects were seated with their hands and lower limbs secured into an apparatus constraining the muscles to isometric contractions. The authors induced two types of controlled movements (perturbations externally applied directly to the sensors and perturbations produced as a result of body movement), thereby eliciting more than 300 controlled isometric contractions with and without movement artefacts. Seven healthy male subjects and five healthy female subjects have participated in the experiment. The idea was to produce forceful perturbations, which are typically encountered by subjects in work and sport environments. The researchers investigated the existence of correlations between the attenuation rates of the data from the accelerometer sensors and the EMG measurements, and based on their observation, determined the appropriate corner frequencies of a Butterworth band-pass filer which is then used to remove baseline drifts from the useful measurements.

In summary, whilst proposed approaches suggest the possibility of removing motion artefatcs by employing inertial sensors, the statistics of the motion artefacts are not closely studied. As a result, the justifications for employing the proposed noise removal techniques are not adequate. In this paper we closely investigate the noise statistics and demonstrate how we establish the correlation between the motions affecting the electrodes of a wireless ECG and the motion artefacts included in the useful measurements.

III. Noise Estimation

Suppose we regard the i-th sample of a wireless electrocardiogram, the movement-induced artefacts it contains, and the corresponding sample obtained from an inertia sensor as random variables, **r**, **n**, and **a**, respectively. We remove the index i for the sake of convenience. In case the inertial sensor measures the three dimensional movement or acceleration affecting the electrocardiogram electrodes, **a** is a vector containing three random variables:

$$\mathbf{a} = (\mathbf{a}_x, \mathbf{a}_y, \mathbf{a}_z)^\intercal \tag{1}$$

Our aim is to estimate **n** in terms of **a**:

$$\hat{\mathbf{n}} = g(\mathbf{a}) \tag{2}$$

Different optimisation strategies can be sought in order to determine the function which best estimates the noise in Equation 2. The ideal estimator is the one in which $\hat{\mathbf{n}}$ coincides with the unknown **n**. This, of course, is almost always an impossible endeavour and any estimate will result in an error:

$$\mathbf{e}(\mathbf{a}) = \mathbf{n} - g(\mathbf{a}) \tag{3}$$

One strategy would be to select g so as to minimise some aspect of this error, such as minimising the mean square error:

$$\sigma^2(\mathbf{a}) = E\left[\mathbf{e}^2(\mathbf{a})\right] \tag{4}$$

To simplify the evaluation of Equation 4, we can employ conditional probability, recalling:

$$E[\mathbf{x}] = E_y\left[E_x[\mathbf{x}|y]\right] \tag{5}$$

where the conditional **x** in the above equation represents the expected value of **x** given an instance, y, of the random variable **y**. For our case, this amounts to actual measurements (observations) made by the three dimensional inertial sensor. Hence, the mean square error can be expressed as:

$$\sigma^2(\mathbf{a}) = E_a\left[E_n\left[(\mathbf{n} - g(a))^2 |a\right]\right] \tag{6}$$

where the inner expectation is with respect to **n** fixing $\mathbf{a} = a$ and the outer expectation is with respect to **a**. As a result, we have:

$$\sigma^2(\mathbf{a}) = \int_{-\infty}^{\infty} E\left[(\mathbf{n} - g(a))^2 |a\right] f(a) da \tag{7}$$

where $f(a)$ is the probability density function of **a**. In order to minimise the error, the above expression should be differentiated with respect to $g(a)$. As can be seen, all the terms within the integral are positive values. Moreover, as $g(a)$ appears only in the integrand term, minimising the estimation error is equivalent to minimising the conditional expected error with respect to $g(a)$:

$$\frac{\partial}{\partial g(a)} E\left[(\mathbf{n} - g(a))^2 |a\right] = 0 \tag{8}$$

The evaluation of the last term yields:

$$E[\mathbf{n}|a] = E[g(a)|a] \tag{9}$$

$E[g(a)|a] = g(a)$ for all a, because a is already given. Therefore, it can be concluded that the optimal estimator of **n** is given as:

$$\hat{\mathbf{n}} = g(\mathbf{a}) = E[\mathbf{n}|\mathbf{a}] \tag{10}$$

From Equation 12, it is clear that **n** and **a** should be correlated for the best estimator to yield a meaningful result. In the next section, we shall demonstrate how we attempted to evaluate the existence of correlation between **n** and **a** for different types of movements.

IV. Establishing Motion Artefacts Statistics

As we already stated in Section I, we employed a 3D accelerometer to reason about the movements affecting the electrodes of a wireless ECG. In one of our experiments, we took measurements from four young and healthy subjects (between 22 and 35 years), two men and two women. These subjects were asked to make five different types of movements: walking and running on a flat surface, climbing up and climbing down a staircase, and outdoor cycling. For each movement type, the measurement lasted 3 minutes. The ECG was sampled at $300\,\mathrm{Hz}$ and $512\,\mathrm{Hz}$. We employed the Shimmer platform [6] consisting of a 5-lead wireless ECG, a 3D accelerometer, a 3D gyroscope, and a 3D magnetometer. The advantage of using this platform was that all the sensors could be synchronised and sampled at the same frequency. Its disadvantage was that the location from where the inertial measurements were taken and the location where the electrodes were actually placed were different — however, this distance was less than 5 cm.

In order to establish the correlation between **n** and **a**, we took into account knowledge of cardiac action potentials (ref. to Fig. 2). The longest interval where there should be zero potentials in a normal ECG measurement is the interval between the P-wave and the T-wave of two consecutive heartbeats. If, however, this interval contains non-zero potentials, this must be due to the effect of motion artefacts — included, of course, is also the noise arising from other sources but, during movement, the movement artefacts are dominant. Consequently, the samples of this region of the ECG measurement can be correlated with the samples of the 3D accelerometer of the same duration and interval to establish a relationship between the motion artefacts and the motion of the user. Furthermore, if we assume that for a short duration (equalling approximately the duration of a single heartbeat) the motion artefacts are, statistically speaking, stationary in a wide sense, then, it is possible to take the samples between the T and the P waves as representatives of the motion artefacts contained in the interval between the peaks of two heartbeats (i.e., the RR interval). This is a plausible assumption considering the relatively high sampling rate. By comparison, human beings' normal movement is below $3\,\mathrm{m/s}$. The region of the ECG measurement from where we extracted samples to establish the statistics of **n** is shown in Fig. 3.

We observed that the strength of correlation between the motion artefacts inside the noisy ECG and the motion vibrating the electrodes as well as the motion affecting the electrical characteristics of the skin (i.e., the motion measured by the inertial sensors) depended on many factors, including:

- the type of movement,

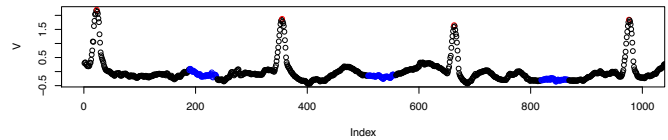

Fig. 3: The interval between the T-wave and the P-wave of two consecutive heartbeats can be used to establish a correlation between **n** and **a**.

TABLE I: The correlation between the noise statistics and the samples of the 3D accelerometer for ten arbitrarily selected heartbeats. The subject was running.

	$\mathrm{cor}(n, a_x)$	$\mathrm{cor}(n, a_y)$	$\mathrm{cor}(n, a_z)$	$\mathrm{cor}(a_x, a_y)$	$\mathrm{cor}(a_x, a_z)$	$\mathrm{cor}(a_y, a_z)$
1	0.28151	0.19357	0.03879	0.51320	-0.49442	-0.93110
2	-0.96326	-0.88885	-0.55308	0.83758	0.64575	0.23781
3	0.77703	0.75001	0.13232	0.88615	0.20844	0.53813
4	0.08275	0.16051	-0.23802	-0.00130	-0.56141	-0.49459
5	-0.55031	-0.57711	0.55772	0.96389	-0.70878	-0.82598
6	-0.46170	0.55012	-0.44659	-0.76931	0.59393	-0.80759
7	0.09984	0.11609	0.21568	0.82242	-0.90326	-0.86043
8	0.05557	-0.52623	0.03587	0.37923	-0.75668	-0.49001
9	-0.43598	0.42745	-0.15834	0.53287	-0.32561	-0.48014
10	-0.01502	-0.85005	0.75000	0.43090	-0.05384	-0.60290

- the number of samples extracted from a single heartbeat to model the noise, and
- the irregularity of the relative location and duration of the RR-intervals.

Table I - V provide an overview of the correlations we computed for ten arbitrarily selected RR-intervals for the five different movement types we have investigated. A careful review of the tables reveals that, in most cases, there is indeed a correlation between **n** and **a**. For some movements (walking and running), the correlation is both consistent and strong whilst for other movements (climbing up and down a staircase) the correlation is sometimes strong and sometimes weak. The weakness in correlation can be due to two factors:

- the relative position of the 3D accelerometer.
- the selection of samples to model the noise.

Since the place where we deployed the electrodes of the wireless ECG and the place where the 3D accelerometer was placed were different, the motion which was measured by the accelerometer may not accurately represent the motion affecting the interface between the electrodes and the skin. This might have resulted in an error in the relationship between **n** and **a**. This error can be corrected by directly embedding accelerometers into the electrodes rather than placing a single accelerometer inside the ECG platform. Secondly, since determining the precise zero-potential interval between the T-wave and the P-wave was difficult, the selection of samples in order to construct the noise statistics was inaccurate. Therefore, this step introduced an additional source of error.

V. Linear Estimation of Motion Artefacts

An interesting aspect which can be observed in the correlation tables is that where there is a strong correlation

TABLE II: The correlation between the noise statistics and the samples of the 3D accelerometer for ten arbitrarily selected heartbeats. The subject was cycling.

	$\mathrm{cor}(n, a_x)$	$\mathrm{cor}(n, a_y)$	$\mathrm{cor}(n, a_z)$	$\mathrm{cor}(a_x, a_y)$	$\mathrm{cor}(a_x, a_z)$	$\mathrm{cor}(a_y, a_z)$
1	-0.76675	0.81227	0.00706	-0.50231	-0.00949	-0.02622
2	-0.37038	0.48820	-0.00878	-0.96535	-0.75564	0.67304
3	0.10053	-0.24157	-0.07299	0.62418	0.07965	0.71116
4	-0.81498	0.69464	0.71517	-0.77342	-0.70575	0.62643
5	-0.00894	0.63618	-0.62584	-0.54647	0.16896	-0.20959
6	-0.80260	0.76180	0.90998	-0.76977	-0.78039	0.84346
7	0.61210	0.39157	-0.24771	0.87257	-0.35673	-0.54229
8	-0.18066	-0.86390	0.45936	0.00495	-0.70125	-0.25488
9	-0.09962	-0.47031	-0.37307	0.39526	0.62520	0.79373
10	-0.49564	-0.69793	0.61691	0.56415	-0.58318	-0.28431

TABLE III: The correlation between the noise statistics and the samples of the 3D accelerometer for ten arbitrarily selected heartbeats. The subject was climbing up a staircase with a normal pace.

	$\mathrm{cor}(n, a_x)$	$\mathrm{cor}(n, a_y)$	$\mathrm{cor}(n, a_z)$	$\mathrm{cor}(a_x, a_y)$	$\mathrm{cor}(a_x, a_z)$	$\mathrm{cor}(a_y, a_z)$
1	-0.86747	-0.87528	-0.83687	0.82103	0.88619	0.93908
2	-0.29359	0.49807	0.46887	0.51717	-0.66475	0.06919
3	0.28992	0.33520	-0.69191	-0.51939	-0.17473	-0.61713
4	-0.13454	0.11926	0.07344	-0.39677	-0.75729	0.70862
5	0.40654	0.98276	0.48867	0.35570	0.23745	0.52711
6	0.15440	0.26972	0.34084	-0.31490	0.30057	0.30988
7	0.45577	-0.26626	0.60263	0.62404	0.41516	-0.11907
8	0.48928	-0.83430	-0.33350	-0.34778	-0.32674	0.55719
9	0.76912	0.86772	0.63495	0.58755	0.39165	0.80984
10	-0.61558	-0.34990	0.83249	0.87445	-0.55597	-0.16838

TABLE IV: The correlation between the noise statistics and the samples of the 3D accelerometer for ten arbitrarily selected heartbeats. The subject was climbing down a staircase with a normal pace.

	$\mathrm{cor}(n, a_x)$	$\mathrm{cor}(n, a_y)$	$\mathrm{cor}(n, a_z)$	$\mathrm{cor}(a_x, a_y)$	$\mathrm{cor}(a_x, a_z)$	$\mathrm{cor}(a_y, a_z)$
1	0.62865	0.60970	-0.05609	0.47369	0.07333	-0.26272
2	-0.70519	-0.15077	0.09825	-0.05369	-0.32781	0.84039
3	0.80880	-0.60403	-0.91552	-0.63818	-0.80708	0.67456
4	-0.00202	-0.72297	0.70027	0.65894	-0.20421	-0.63026
5	0.05400	-0.31185	-0.57604	-0.18354	-0.22869	0.57886
6	-0.41010	-0.51737	-0.25168	0.34219	0.24290	0.40867
7	-0.86583	0.69560	-0.19689	-0.63312	0.28682	-0.05991
8	0.03727	-0.32002	0.30859	-0.72125	0.44999	-0.67733
9	0.26127	-0.48030	-0.40525	-0.05285	-0.64888	0.67246
10	-0.29800	0.85199	-0.61287	-0.51879	0.87137	-0.80886

TABLE V: The correlation between the noise statistics and the samples of the 3D accelerometer for ten arbitrarily selected heartbeats. The subject was walking at a normal pace.

	$\mathrm{cor}(n, a_x)$	$\mathrm{cor}(n, a_y)$	$\mathrm{cor}(n, a_z)$	$\mathrm{cor}(a_x, a_y)$	$\mathrm{cor}(a_x, a_z)$	$\mathrm{cor}(a_y, a_z)$
1	0.22073	-0.03518	0.88518	0.08072	0.19229	0.00312
2	-0.81243	0.02660	-0.91760	0.25399	0.95237	0.18346
3	0.97261	-0.21160	-0.95296	-0.26227	-0.92907	0.04188
4	-0.02154	0.10071	-0.07446	0.92210	-0.09339	-0.04772
5	0.80465	0.56259	0.34071	0.46069	0.64155	-0.34217
6	0.57602	0.39250	-0.71638	-0.26870	-0.79659	0.07442
7	0.56530	0.06831	0.48544	-0.36285	0.15962	0.65284
8	-0.03586	0.42871	0.45617	-0.01965	-0.01589	0.94859
9	0.43325	-0.04453	-0.47496	-0.00741	-0.33814	0.12651
10	-0.72422	-0.96302	-0.95124	0.69666	0.77569	0.95945

TABLE VI: The different expected values computed for determining the weights of the linear equation to estimate the motion artefacts for ten arbitrarily selected heartbeats. The subject was running.

	$E[n \cdot a_x]$	$E[n \cdot a_y]$	$E[n \cdot a_z]$	$E[a_x \cdot a_x]$	$E[a_y \cdot a_y]$	$E[a_z \cdot a_z]$	$E[a_x \cdot a_y]$	$E[a_x \cdot a_z]$	$E[a_y \cdot a_z]$
1	0.44884	1.60280	0.17021	4.40331	56.73510	0.93270	15.62343	1.55410	5.27486
2	-0.11362	-0.08664	0.00193	2.93598	133.51362	3.97658	17.24425	2.89793	22.15249
3	0.16011	0.40036	0.03811	8.66106	49.03542	1.41439	20.35959	3.20658	7.86898
4	-0.16468	-0.43337	-0.21509	69.37458	300.08602	24.53827	129.73049	-5.21431	5.42421
5	-0.48939	-1.33299	-0.06728	2.79355	22.20229	0.52538	7.74997	0.02507	-0.36802
6	1.93387	14.48193	-1.23666	10.60998	316.34888	33.20575	45.22699	4.52543	-20.23937
7	-0.43544	-1.49193	0.04972	2.94134	31.34125	0.31859	9.21887	-0.61119	-1.74033
8	-0.53114	-1.77837	-0.07309	73.91226	247.97767	63.37908	115.92153	-15.07785	-2.40582
9	0.69969	2.40465	0.06282	6.28027	68.36240	0.26493	20.36013	0.51463	1.54203
10	0.70362	2.17661	0.88808	4.98978	93.38573	22.33072	18.03825	3.00098	-3.32090

between $\mathbf{n}$ and $\mathbf{a}$, there is also a strong correlation between the different axes of the accelerometer. If we assume that $\mathbf{n}$ can be estimated as a linear combination of the three dimensional acceleration:

$$\hat{\mathbf{n}} = \alpha_x \mathbf{a}_x + \alpha_y \mathbf{a}_y + \alpha_z \mathbf{a}_z \tag{11}$$

then, it is possible to determine the proper weights (α_i) by making use of the correlation tables. This is because, the mean square error in Equation 4 can be expressed as:

$$E\left[\mathbf{e}\left(\mathbf{a}\right)^2\right] = E\left\{\left[\mathbf{n} - \left(\alpha_x \mathbf{a}_x + \alpha_y \mathbf{a}_y + \alpha_z \mathbf{a}_z\right)\right]^2\right\} \tag{12}$$

In order to determine the optimal α_i, we have to differentiate Equation 12 with respect to α_i and set the result to zero. This leads to the following Equation[1]:

$$\begin{aligned} E\left\{\mathbf{n}\mathbf{a}_x\right\} &= \alpha_x E\left\{\mathbf{a}_x^2\right\} + \alpha_y E\left\{\mathbf{a}_y \mathbf{a}_x\right\} + \alpha_z E\left\{\mathbf{a}_z \mathbf{a}_x\right\} \\ E\left\{\mathbf{n}\mathbf{a}_y\right\} &= \alpha_x E\left\{\mathbf{a}_x \mathbf{a}_y\right\} + \alpha_y E\left\{\mathbf{a}_y^2\right\} + \alpha_z E\left\{\mathbf{a}_z \mathbf{a}_y\right\} \\ E\left\{\mathbf{n}\mathbf{a}_z\right\} &= \alpha_x E\left\{\mathbf{a}_x \mathbf{a}_z\right\} + \alpha_y E\left\{\mathbf{a}_y \mathbf{a}_z\right\} + \alpha_z E\left\{\mathbf{a}_z^2\right\} \end{aligned} \tag{13}$$

Letting $E\left\{\mathbf{n}\mathbf{a}_i\right\} = R_{ni}$ and $E\left\{\mathbf{a}_i \mathbf{a}_j\right\} = R_{ij}$, we can express the above equation in a matrix form as follows:

$$\begin{bmatrix} R_{nx} \\ R_{ny} \\ R_{nz} \end{bmatrix} = \begin{bmatrix} R_{xx} & R_{xy} & R_{xz} \\ R_{yx} & R_{yy} & R_{yz} \\ R_{zx} & R_{zy} & R_{zz} \end{bmatrix} \begin{bmatrix} \alpha_x \\ \alpha_y \\ \alpha_z \end{bmatrix} \tag{14}$$

From Equation 14, we can determine the α coefficients by taking the inverse of the square matrix of the right term:

$$\begin{bmatrix} \alpha_x \\ \alpha_y \\ \alpha_z \end{bmatrix} = \begin{bmatrix} R_{xx} & R_{xy} & R_{xz} \\ R_{yx} & R_{yy} & R_{yz} \\ R_{zx} & R_{zy} & R_{zz} \end{bmatrix}^{-1} \begin{bmatrix} R_{nx} \\ R_{ny} \\ R_{nz} \end{bmatrix} \tag{15}$$

Table VI displays the different expected values we computed in order to establish Equation 15 to reason about the motion artefacts when a subject was running. The α values we computed to estimate the motion artefacts are given in Table VII. Figure 4 displays $\hat{\mathbf{n}}$ we estimated using the αs. The figure at the top is the raw estimate whereas the one at the bottom is the smoothed estimate.

[1]The first raw is a result of differentiating Equation 12 with respect to α_x, the second, with respect to α_y, and the third, with respect to α_z.

TABLE VII: The alpha values determined to estimate the noise artefacts for ten arbitrarily selected heartbeats. The subject was running.

	α_x	α_y	α_z
1	0.03354	0.01527	0.04023
2	-0.14828	0.00651	0.07227
3	-0.09030	0.07912	-0.20850
4	-0.00378	0.00037	-0.00965
5	0.05428	-0.08210	-0.18817
6	-0.02664	0.04936	-0.00353
7	-0.06159	-0.03930	-0.17680
8	0.01684	-0.01502	0.00228
9	-0.09124	0.06101	0.05923
10	0.13748	-0.00250	0.02092

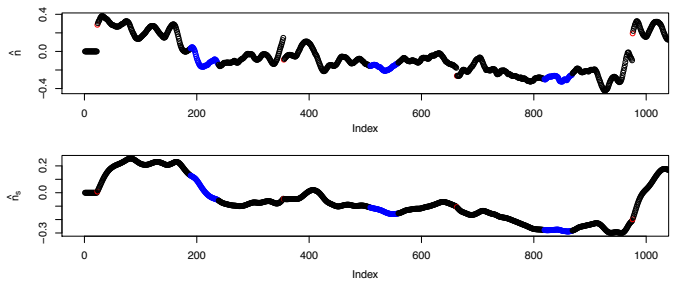

Fig. 4: The interval between the T-wave and the P-wave of two consecutive heartbeats can be used to establish a correlation between **n** and **a**.

VI. Conclusion and future Work

In this paper we attempted to establish the statistics of motion artefacts included in the measurements of a wireless ECG during mobility. We employed a 3D accelerometer and knowledge of cardiac action potentials for our task and our analysis and modelling relied on measurements taken from four healthy adults undertaking five different types of everyday movements: walking, running, cycling, and climbing up and down a staircase.

Hence, in the measurement of a normal electrocardiogram of an adult, a single heartbeat consists of a sequence of P-wave, a QRS wave complex, and a T-wave. The intervals between these waves comprise of zero potentials. Of these, the longest interval is the interval between a T-wave and a P-wave of two consecutive heartbeats. If, during motion, this interval contains considerable non-zero potentials, we argued that this must be a result of motion artefacts. We manually located these intervals in our datasets and extracted samples to construct the statistics of motion artefacts and correlated them with the samples of the measurements from the 3D accelerometers corresponding to these same intervals. Our initial results suggest that there is a correlation between the samples of the motion artefacts and the samples of the 3D accelerometer, but the strength of the correlation differs from sample to sample. For our case, the movement type where we observed a strong, consistent correlation was running and the movement types where we observed weak, unpredictable correlation were climbing up and down a staircase.

After we proved the existence of correlation, we estimated the motion artefacts included in the noisy ECG measurements as a linear combination of the three dimensional accelerations affecting the electrodes of the wireless ECG. We used linear mean square estimation to determine the optimal weights of our linear equation. What remains is to closely investigate the probability density function of the noise artefacts and determine the optimal estimator in order to remove them from the noisy ECG measurements. This will be our future work.

Acknowledgement

This work has been partially funded by the German Research Foundation (DFG) under the project agreement: DA 1211/7-1 (Roreyban). The author also wishes to express his appreciation of the winter 2017/18 Prediction and Estimation Technique class at the Technische Univerität Dresden for their independent verification of the proposed approach. Special thanks goes to Til Jasper Ulrich and Weijie Wu.

References

[1] W. Dargie, *Principles and Applications of Ubiquitous Sensing*. John Wiley & Sons, 2017.

[2] M. E. Kiani, A. Al-Ali, R. Coverston, G. Mason, and F. Robertson, "Physiological sensor combination," June 14 2016. US Patent 9,364,181.

[3] K. Luo, J. Li, and J. Wu, "A dynamic compression scheme for energy-efficient real-time wireless electrocardiogram biosensors," *IEEE Transactions on Instrumentation and Measurement*, vol. 63, no. 9, pp. 2160–2169, 2014.

[4] R. Gupta and M. Mitra, "Wireless electrocardiogram transmission in ism band: an approach towards telecardiology," *Journal of medical systems*, vol. 38, no. 10, p. 90, 2014.

[5] M. Elgendi, B. Eskofier, S. Dokos, and D. Abbott, "Revisiting qrs detection methodologies for portable, wearable, battery-operated, and wireless ecg systems," *PloS one*, vol. 9, no. 1, p. e84018, 2014.

[6] A. Burns, B. R. Greene, M. J. McGrath, T. J. O'Shea, B. Kuris, S. M. Ayer, F. Stroiescu, and V. Cionca, "Shimmer^{TM}–a wireless sensor platform for noninvasive biomedical research," *IEEE Sensors Journal*, vol. 10, no. 9, pp. 1527–1534, 2010.

[7] M. Khayatzadeh, X. Zhang, J. Tan, W.-S. Liew, and Y. Lian, "A 0.7-v 17.4-/spl mu/w 3-lead wireless ecg soc," *IEEE transactions on biomedical circuits and systems*, vol. 7, no. 5, pp. 583–592, 2013.

[8] F. Massé, M. V. Bussel, A. Serteyn, J. Arends, and J. Penders, "Miniaturized wireless ecg monitor for real-time detection of epileptic seizures," *ACM Transactions on Embedded Computing Systems (TECS)*, vol. 12, no. 4, p. 102, 2013.

[9] W. Dargie, "A stochastic fusion technique for removing motion artefacts from the measurements of a wireless ecg," in *Multisensor Fusion and Integration for Intelligent Systems (MFI), 2016 IEEE International Conference on*, pp. 449–454, IEEE, 2016.

[10] M. Li, Y. Cui, and J. Yang, "Automatic removal of ocular artifact from eeg with dwt and ica method," *Applied Mathematics & Information Sciences*, vol. 7, no. 2, p. 809, 2013.

[11] M. Kaur, B. Singh, *et al.*, "Comparison of different approaches for removal of baseline wander from ecg signal," in *Proceedings of the International Conference & Workshop on Emerging Trends in Technology*, pp. 1290–1294, ACM, 2011.

[12] D. Tong, K. Bartels, and K. Honeyager, "Adaptive reduction of motion artifact in the electrocardiogram," in *EMBS/BMES Conference*, (Houston, TX, USA), 2002.

[13] I. Romero, T. Berset, D. Buxi, L. Brown, J. Pernder, S. Kim, N. Van Helleputte, H. Kim, C. Van Hoof, and F. Yazicioglu, "Motion artifact reduction in ambulatory ecg monitoring: An integrated system approach," in *Proceedings of Wireless Health*, (San Diego, CA, USA), 2011.

[14] C. J. De Luca, L. D. Gilmore, M. Kuznetsov, and S. H. Roy, "Filtering the surface emg signal: Movement artifact and baseline noise contamination," *Journal of biomechanics*, vol. 43, no. 8, pp. 1573–1579, 2010.